Applied Catalysis B: Environmental 300 (2022) 120732

Contents lists available at ScienceDirect

Applied Catalysis B: Environmental

journal homepage: www.elsevier.com/locate/apcatb

Conjugated polymers templated carbonization to design N, S co-doped finely tunable carbon for enhanced synergistic catalysis

Abdellah Ait El Fakir [a,b,*], Zakaria Anfar [a,b,c,1], Mohamed Enneiymy [b,c], Amane Jada [b,c,*], Noureddine El Alem [a]

[a] Laboratory of Materials & Environment (LME), Ibn Zohr University, Agadir 80000, Morocco
[b] Institute of Materials Science of Mulhouse (IS2M), Haute Alsace University, Mulhouse 68100, France
[c] Strasbourg University, Strasbourg 67081, France

ARTICLE INFO

Keywords:
N, S doped carbon
Conjugated polymers
Direct carbonization
Persulfate activation
Synergistic effect

ABSTRACT

Efficient generation of $^1O_2$ nonradical species from persulfate (PS) is demonstrated during heterogeneous catalysis systems based on the use of new Nitrogen and Sulfur doped carbons (NC, SC and NSC), as prepared by direct carbonization of polyaniline/polythiophene conjugated polymers at 800 °C. Complete organic molecules degradations were achieved with high mineralization rate (~70%) for all systems, over a wide pH range (2.6~9.5) in the presence of PS. Interestingly, the synergistic effect occurring between the N-Graphitic and the S-Thiophenic sites, modulates the surface electron density toward basic carbon structure (N~4.76 at% and S~3.87 at%, with S_{BET}~251 $m^2\ g^{-1}$), leads to increases of the adsorption abilities and the reaction rate constant (from 0.076 to 0.338 min^{-1}), and boosts the carbocatalyst' stability. Our discovery sheds new light on new systems promoting the Fenton-like oxidation process by $^1O_2$ nonradical species, it may be a long-lasting sustainable environmentally strategy for water remediation.

1. Introduction

In the wastewater treatment, the advanced oxidation processes (AOPs), as compared to the traditional physical, biological and chemical technologies, were found to be adequate and more efficient, for the organic pollutants removal [1]. The use of the persulfate-Based Advanced Oxidation Processes (SR-AOPs) in the wastewater treatment, is more promising, due to the high decomposition capacity to radicals of these chemical compounds [2–5]. In fact, sulfate radicals ($SO_4^{\bullet-}$), which are generated from the peroxymonosulfate (PMS) or the persulfate (PS) activation, during the catalytic process, are more selective than hydroxyl radicals ($OH^{\bullet}$), as resulting from their higher oxidation potential ($SO_4^{\bullet-}$ 2.5–3.1 V vs $OH^{\bullet}$ 2.7 V), and their longer half-life (30–40 μs) in organic pollutants degradation, leading hence to better mineralization of the pollutants to CO_2 and H_2O [3,6–9]. In addition, the PS could be activated by various approaches such as catalysis by transition metal ions, heating, UV irradiation, metal oxides and carbonaceous materials (carbocatalysts) [10–16]. Carbocatalysts or metal-free catalysts such as carbon nanotubes, graphene and porous carbon have received lot of attentions in recent years, due to their high surface area and their high adsorption capacity. These carbon materials are synthesized through simple pyrolysis processes, and carry large amounts of oxygen-containing functional groups, which were also involved in the adsorption of contaminants and PS activation [17,18]. Then, the carbocatalysts can effectively hinder the formation of potential secondary contaminants that may result from toxic metals leaching [2,3]. In addition, metal-free catalysts synthesis are recognized as cheap and environmentally friendly protocols [10,12,13,19–21]. On the other hand, carbon based materials are known by their catalytic activity which can be further improved by the doping process with heteroatoms [12,13,20,22–28]. Doping carbon matrices with heteroatoms (i.e. N, S, B, P) is simple and feasible strategy, allowing hence point defects creation, and leading to carbocatalysts having higher adsorption capacity and catalytic performance [29]. It should be noted that the dopant having higher electronegativity, in comparison to carbon, can change the electronic distribution, and the chemical inertia, of the carbon matrix [29]. In particular, the co-doping with many heteroatoms

* Corresponding authors at: Institute of Materials Science of Mulhouse (IS2M), Haute Alsace University, Mulhouse 68100, France.
E-mail addresses: aitelfakir.abdellah@gmail.com (A. Ait El Fakir), amane.jada@uha.fr (A. Jada).
[1] Present Address: Institute of Chemistry & Biology of Membranes & Nano-objects (UMR5248 CBMN), CNRS, University of Bordeaux, Institut Polytechnique Bordeaux 2 rue Robert Escarpit, Pessac 33607, France.

https://doi.org/10.1016/j.apcatb.2021.120732
Received 11 June 2021; Received in revised form 9 September 2021; Accepted 14 September 2021
Available online 17 September 2021

(example N, S) can lead to a synergistic effect which results from the multiple electronic distributions appearing in the carbon matrix [23–25, 29–31]. In addition, several experimental and theoretical studies in the literature, have shown that the co-doped carbocatalysts exhibit better catalytic performance, than those singly doped with N or S heteroatom, due to a cooperative and synergistic effect (Table S1) [24,25,27,31,32]. Recently, most of the doped, and co-doped carbon materials, were synthesized by the addition of external heteroatoms sources (for example, melamine, ammonium nitrate and urea as sources of N, and Thiourea for S heteroatom) [11,25,27,32]. However, the heteroatoms doped carbocatalysts surface by using external sources can lead to a decrease of the surface area, and the heteroatoms leaching during the catalytic process, as resulting from the weak interaction occurring between the heteroatoms and the carbon basal surface [22,33,34]. Further, the preparation processes of the heteroatoms doped carbon material by addition of external heteroatoms sources, generally suffered from complicated technology and the instability of doping heteroatoms [14,33,34]. These problems could be solved by one-pot synthesis process of heteroatoms doped carbocatalysts by carbonization of precursors containing initially heteroatoms in their structures. Therefore, an easy, available and inexpensive synthesis is highly desirable.

Conjugated polymers such as, Polyaniline (PANI) and Polythio phene (PTh) are metal-free materials composed of carbon, heteroatoms and hydrogen [10,35–37]. These polymers are widely used in many fields, including biosensors, adsorbent materials, supercapacitors, due to their high conductivity, ease of their synthesis, their electrochemical activity, the stability of the heteroatoms contained in their conjugated system, and their non-toxicity [35–37]. Based on their characteristics and their high carbon and heteroatom contents, we have recently used conductive polymers, as metal-free catalysts, in the activation of PS [10]. Therefore, the one-pot synthesis of heteroatoms doped carbon materials from conjugated polymers can be carried out at high temperatures, without adding external heteroatoms sources, achieving hence the reconstruction of the N or S doped carbon in situ [14,22,33, 34]. It is noteworthy to note that this doping method will not only simplify the synthesis procedure, but it will also generate a significant amount of the higher reactivity active sites for the PS and the PMS activation [14,22,33,34].

In the present work, we have brought a new insight into the one-pot synthesis of N, S co-doped carbon (NSC) from the carbonization of conjugated copolymer polyaniline-co-polythiophene (PANI-co-PTh), which was synthesized from two monomers such as aniline as a source of N and thiophene as a source of S. Further, in order to give evidence of the cooperative and synergistic effects occurring in the N, S co-doped carbon (NSC), in comparison to individual N or S doped carbon, we have also prepared the N doped carbon (NC), and the S doped carbon (SC), from direct carbonization of PANI and PTh, respectively. Regarding the organic pollutants, and in order to assess the catalytic activity of PS activation, we have selected Orange G, Rhodamine B, and BPA, as target contaminants which are widely generated and difficult to degrade. In addition, the influence of various parameters that may affect the organic pollutants degradation process have been studied and discussed in detail. The PS activation mechanism has also been elucidated in trapping and Electron Paramagnetic Resonance (EPR) experiments.

2. Experimental section

2.1. Chemical's reagents

Aniline and thiophene monomers were purchased from Sigma Aldrich and distilled before their uses. Ammonium persulfate (APS, $(NH_4)_2S_2O_8$), Iron chloride ($FeCl_3$), Chloroform ($CHCl_3$), sodium hydroxide (NaOH), hydrochloric acid (HCl) (37%), L-Histidine, tert-butanol (TBA), ethanol (EtOH), p-benzoquinone (p-BQ), sodium persulfate (PS, $Na_2S_2O_8$, 99%), sodium alginate, orange G (OG), bisphenol A (BPA), and rhodamine B (RhB), were provided by Sigma-Aldrich and were used as received. The pH values of the solutions were adjusted by using HCl and NaOH standard aqueous solutions (Merck Millipore).

2.2. Preparation of carbocatalysts NSC, NC and SC

Firstly, the (PANI) was prepared following a simple polymerization method as shown in our previous work [10]. The Polythiophene (PTh) was prepared by using simple polymerization process based on the thiophene monomer oxidation with a known ratio (thiophene/$FeCl_3$). Hence, a solution of thiophene monomer (1 mL in 30 mL of anhydrous chloroform ($CHCl_3$)), then a solution of $FeCl_3$ (6.5 mg, in 20 mL of anhydrous $CHCl_3$) was added dropwise to the monomer solution. Subsequently, the resulting mixed solution was stirred at room temperature for 24 h. Finally, the product was collected by vacuum filtration, washed several times with deionised water and absolute ethanol. Finally, the obtained product was dried at 60 °C in a vacuum oven for 12 h. Regarding the copolymer polyaniline-co-polythiophene (PANI-co-PTh), it was obtained by the same protocol used to synthesize polymer PTh, replacing the thiophene monomer with a mixture of two monomers (thiophene (0.5 mL) and aniline (0.5 mL)).

To obtain the Nitrogen and/or Sulfur doped carbons the polymers PANI, PTh and PTh-co-PANI were calcined at 800 °C in a tubular furnace with the heating rate of 5 °C min^{-1} under nitrogen argon atmosphere for 3 h. Then, after pyrolysis the carbocatalysts obtained were collected, grinded and washed successively with plenty of Milli-Q water and acetone and finally dried at 50 °C for 24 h. The final products were denoted, respectively, NC (Scheme 1a), SC (c), and NSC (b).

2.3. Preparation of NSC@Alginate catalysts

The hydrogel beads NSC@Alginate were prepared according to the following protocol: 100 mg of alginate powder was dissolved in 20 mL of deionized water and stirred at constant agitation for 4 h. Then, 100 mg of NSC was added to the mixture and stirred at constant agitation for 3 h. On another hand, $CaCl_2$ aqueous solution (0.1 M) was prepared and placed in a beaker with constant stirring. Thus, the hydrogel beads were prepared by adding the mixture NSC/alginate to the $CaCl_2$ aqueous solution dropwise using a pump. Note that in the last preparation step, each droplet of the NSC/alginate was in contact with the Ca^{2+} ions, leading hence to the formation of spherical hydrogel beads having core-shell like structure, i.e., a core made of NSC catalyst covered by a shell consisting of alginate-Ca^{2+}. Finally, the obtained hydrogel beads were washed with deionized water and stored in a watery medium.

2.4. Characterization

The surface chemical structures of the prepared materials were studied by X-ray Photoelectrons Spectroscopy (XPS) method, and by using XPS VG SCIENTA, Model SES-200. The morphologies of the various prepared catalysts were obtained by Scanning Electron Microscopy (SEM, FEI, model Quanta 400) and Transmission Electron Microscopy (TEM, Philips CM 200). Raman spectra were obtained using DXR™ 2, Thermo Fisher Scientific apparatus operating in the range of 800–2200 cm^{-1} with a 532 nm wavelength incident laser light. The crystalline structures of the hard carbon products were characterized by PANalytical MPD X'Pert Pro diffractometer operating with Cu Kα radiation ($\lambda = 0.15418$ nm). The surface area and porous structure were analyzed by nitrogen adsorption–desorption measurements by using Micrometrics Analyzer, ASAP 2020 instrument.

2.5. Catalytic activity evaluation

The PS activation performances by the NSC, NC and SC carbocatalysts were evaluated via batch experiments, where OG, RhB and BPA were selected as target organic pollutants. Thus, in a typical test, 50 mL of

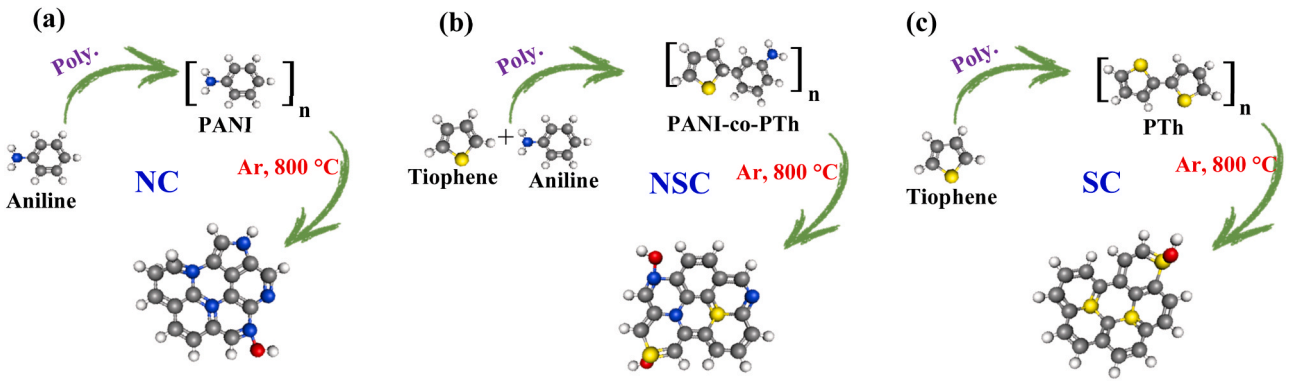

Scheme 1. Schematic illustration of the synthesis of NC (a), NSC (b) and SC (c) carbocatalysts.

organic pollutants concentration aqueous solution ([OG] = 50 mg L^{-1}, [RhB] = 20 mg L^{-1}, [BPA] = 10 mg L^{-1}) was continuously agitated with 0.2 g L^{-1} of carbocatalyst, and 4 mM of PS, for a contact time of 24 min. During the test, at specific time intervals, 2 mL sample volumes were withdrawn and then filtered through filter membrane (0.45 μm, nylon). Further, in order to identify the reactive oxygen species generated in the catalytic reaction, different quenching reagents (EtOH, TBA, L-Histidine and p-BQ) were used to determine the active species in the carbocatalyst/PS systems. Thus, EtOH was employed to scavenge both $SO_4^{\bullet-}$ and $OH^{\bullet}$, while TBA was selected to verify the presence of $OH^{\bullet}$ radicals, and L-histidine and p-BQ were used as $^1O_2$ and $O_2^{\bullet-}$ scavengers, respectively. The carbocatalyst reusability was assessed by recovering it by vacuum filtering from the reaction solution, then it was washed three times by EtOH and deionized water. Subsequently, the recovered carbocatalyst was dried and reused for OG degradation tests. Residual concentrations and calibration curves of OG, RhB and BPA aqueous solutions, were determined by absorbance measurements by using UV-Vis spectrophotometer (6705 UV/Vis JENWAY) at wavelengths λ = 478, 554 and 230 nm, respectively. Further, in order to identify the presence of the ROS in the degradation process, we have conducted in situ electron paramagnetic resonance (EPR) analyzes. Thus, for each analyzed solution, a volume of 50 μL of the reaction medium was transferred in a glass capillary sealed with Crit-O-seal TM, and then placed in an ESR-tube having an outside diameter of 5 mm. In the EPR experiments, N-tert-butyl-α-phenylnitrone (PBN) was used as a spin-trapping agent for $OH^{\bullet}$ and $SO_4^{\bullet-}$, while 2,2,6,6 tetramethylpiperidine (TEMP) was selected as a spin-trapping agent for $^1O_2$. Continuous-wave EPR spectra were recorded at room temperature in aerated medium using an EMX-plus X-band spectrometer (Bruker).

3. Results and discussion

3.1. Catalysts physicochemical structures

The XPS technique was used to study the surface chemistry of the prepared carbocatalysts NSC, NC and SC as shown in Figs. 1a–f. The

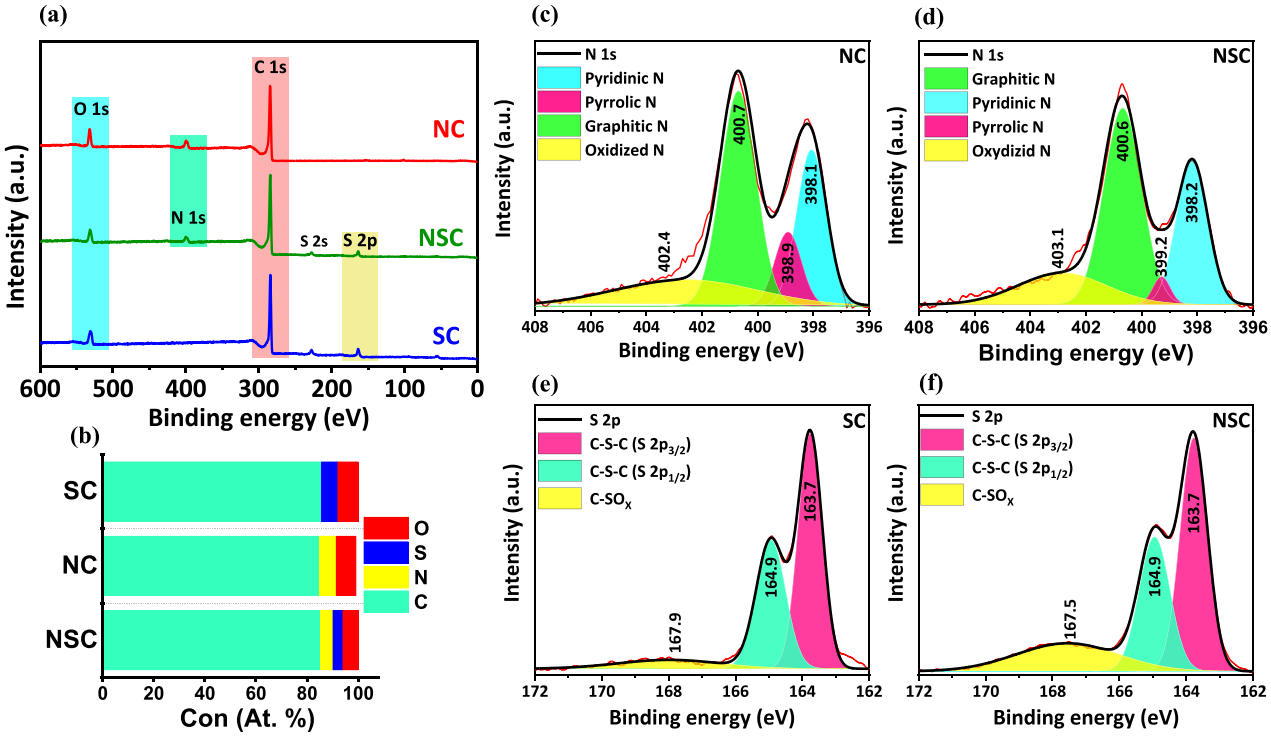

Fig. 1. XPS survey spectra (a) and atomic concentration (b) of NSC, NC and SC Carbocatalysts. High-resolution N 1s spectra of NC (c) and NSC (d). High-resolution S 2p spectra of SC (e), and NSC (f).

survey spectrum of NSC (Fig. 1a) reveals mainly four peaks attributed to C1s, N1s, O1s and S2p, the spectrum of NC (Fig. 1a) contains three main elements C 1s, N 1s and O 1s, and the spectrum of SC (Fig. 1a) includes three elements C 1s, O 1s and S 1s. The XPS results show that the doping of the heteroatoms in the carbon matrix were well achieved, with very interesting percentages as depicted in Table 1. As can be seen, for the NSC material the percentage of heteroatoms is about 8.63% (3.87% S and 4.76% N), the NC material contains about 6.60% N and the SC material contains 6.29% S. Subsequently, high-resolution XPS analyses of C 1s, O 1s, N 1s and S 2p were carried out, to study in detail the chemical bonds within the matrix of the carbocatalysts NSC, NC and SC. The deconvoluted C1s spectra show the existence of four main peaks (Fig. S1a-c), positioned at 284.4, 285.4, 286.8 and 288. 8 eV, attributed to C−C/C═C (sp^3 hybrid carbon and sp^2 graphite-like hybrid carbon), C−N and/or C−S (could be due to sp^2 carbon bound to heteroatoms), C═O (carbonyl or quinine) and O−C═O (carboxyl or ester), respectively [12,14,38]. The deconvolution of O1s from the three samples NC, SC and NSC shows the same components positioned at, 530.0, 531.6 and 533.3 eV assigned C═O, O−C═O and C−O, respectively (Fig. S1d-f) [12]. Concerning the deconvolution of the N 1s peak, of both NSC and NC carbocatalysts, they show four main types of N species (Fig. 1c and d), positioned at 398.1, 399.1, 400.6 and 403.0 eV, and attributed to graphitic N, pyridinic N, pyrrolic N and NOx, respectively [38,39]. The graphitic N, which exhibits significant catalytic activity, as compared to the other N configurations, was found to be the dominant form in the NC and the NSC carbocatalysts (Table 1). The deconvolution of the S 2p peak of both SC and NSC materials, indicates the existence of three peaks (Fig. 1e and f), positioned at 163.7, 164.9 and 167.5 eV, and attributed to C-S-C (S $2p_{3/2}$), C-S-C (S $2p_{1/2}$) and its oxidized forms of C-SOx, respectively [40,41]. It should be noted that the co-presence of N and S in the NSC, with a large atomic percentage, should contribute to promote the catalytic efficiency and to create an important synergistic effect during the persulfate activation process [24,29].

The morphologies of the NSC, NC and SC materials as investigated by SEM are shown in (Fig. 2a−c) and indicate stacked graphitic carbon layers with few pores on the surface of the three carbocatalysts. Further, the NSC, NC and SC catalysts TEM images are depicted in (Fig. 2d−f) and show relatively clear graphitic layers morphology, suggesting hence an enhanced graphitic porous structure, in agreement with the SEM images. The SEM analyzes coupled with the EDS mapping for hydrogel beads NSC@Alg were performed and they are shown in Fig S2. The SEM images of the hydrogel beads show that the NSC carbocatalyst are immobilized inside surrounded by layer of alginate and calcium ions, which gave it a spherical shape bead. In addition, the calcium ions and alginate are concentrated on the beads surface (Fig S2).

Table 1
Physical parameters for the NSC, NC and SC catalysts.

		NSC	NC	SC
XPS	%. O 1s	6.02	7.77	8.01
	%. C 1s	85.35	85.63	85.70
	%. N 1s	4.76	6.60	ND
	%. Graphitic N	49.10	44.72	–
	%. Pyridinic N	34.68	32.91	–
	%. Pyrrolic N	7.66	16.06	–
	%. Oxidized N	8.56	6.30	–
	%. S 2p	3.87	ND	6.29
	%. S I (C-S-C)	92.27	–	96.35
	%. S II (C-SO_x)	7.73	–	3.65
HR-TEM	d_{002} (nm)	0.358	0.346	0.367
BET	S_{BET} ($m^2\ g^{-1}$)	250,638	65,667	306,968
	S_{micro} ($m^2\ g^{-1}$)	212,862	26,640	261,490
	V_{totale} ($cm^3\ g^{-1}$)	0190	0165	0214
	V_{micro} ($cm^3\ g^{-1}$)	0,0810	0,0109	0,1003
Raman	I_G/I_D	1.110	1.119	1.100
XRD	d_{002} (Å)	3.55	3.49	3.65
	L_c(nm)	1.64	1.70	1.61
	L_a (nm)	3.36	3.46	3.27
	N	4.60	4.91	4.39

High resolution TEM images (HR-TEM) were used for the determination of the inter-layer spacings of the NSC, NC and SC samples (Fig. 3a-c). The TEM images show, the disordered bearing structures of the three samples which are consistent with the amorphous carbon's nature. In addition, Fig. 3a−c show that the inter-layer space can be clearly identified at the margins of the samples, after carbonization at high temperature, indicating partial graphitization of the amorphous carbon. The SC sample was found to have a higher inter-layer space of 0.367 nm, as compared to that of the NSC sample, which is about 0.358 nm, whereas the NC sample was found to have the smallest inter-layer space which is about 0.346 nm. The comparison between the inter-layer distance of the various carbocatalysts, indicates clearly that the presence of heteroatoms in these samples causes many structures defects. Moreover, it is obvious that the S atoms, as compared to N atoms lead to the structuration of the carbon into nanosheets and non-homogeneous dispersion. The XRD patterns of SC, NSC and NC carbocatalysts (Fig. 3d), show all two broad (0 0 2) and (1 0 0) peaks, suggesting hence an amorphous nature and disordered carbon [42,43]. Note that the (0 0 2) peak moves to a higher diffraction angle depending on the nature of doping heteroatom (24.34° for SC, 25.05° for NSC and 25.43° for NC) indicating that the d_{002} (inter -layer spacing) decreases due to an increased relative order [44,45]. The calculated d_{002} values are respectively 3.65, 3.55 and 3.49 Å for SC, NSC and NC, respectively (Table 1), confirming that doping the catalyst with S atoms enlarges the inter-layer space due to the larger covalent radius [11]. The thickness and the average width of the graphitic domains, Lc and La, were calculated based on the well-known Scherrer equation, using the FWHM values of (002) [42,43,45]. The number (N) of stacked graphene sheets was obtained by the equation $N = Lc / d_{002}$ (Table 1). As expected Lc, La and N were found to vary depending on the type of doping heteroatom [11]. Thus, the NC sample was found to have the higher Lc, La and N values in a good agreement with the HR-TEM observations. The 2θ diffraction angles were about 43.5° for NSC, NC and SC, and they were attributed to the plane (100) of the amorphous carbon [42,43]. Raman analysis was also carried out to determine the graphitization degree of the carbonaceous materials (Fig. 3e). The spectra of the three carbocatalysts NSC, NC and SC show two characteristic peaks at 1339 and 1596 cm^{-1}, assigned to the D and G bands, respectively. Specifically, the D-band is related to the unordered structure level, while the G-band is related to the internal vibrations of the sp^2 hybridized carbon atoms [38,44]. As shown in Table 1, I_G/I_D represents the ratio of the degree of graphitization to the degree of defect [39,42,43,45]. The NC was found to have the highest ratio (1.01), as compared to the NSC (0.96), and to the SC (0.90), confirming hence, the increase in the graphitic order and the decrease in the defect concentration in the order SC<NSC<NC. These results show that the graphitization is related to the type of doping heteroatom. Thus, S-doping progressively decreases the degree of graphitization and increases the number of defects as well as the inter-layer spaces, which is consistent with the XRD and HR-TEM. The specific surface areas and the pore structures of the various samples were determined using N_2 adsorption-desorption isotherms (Fig. 3f). The curves show IV isotherms type, as well as distinct hysteresis loops which indicate the presence of mesopores various carbocatalysts structures (Fig. S2). In addition, the calculated BET specific surface areas of NSC, SC and NC samples are, 250,6, 306,9 and 65,7 $m^2\ g^{-1}$, respectively. Furthermore, the textural characteristics of the three carbocatalysts, as presented in Table 1, are favorable to the exposure of their active sites leading hence to rapid electron transfer and resulting finally in excellent catalytic activity.

3.2. Degradation performance

The obtained carbocatalysts were evaluated for the degradation of organic pollutants such as orange G (OG), Rhodamine B (RhB) and Bisphenol A (BPA), by using persulfate as oxidant. The catalytic and adsorption performance of NSC, NC and SC towards the OG pollutant, are

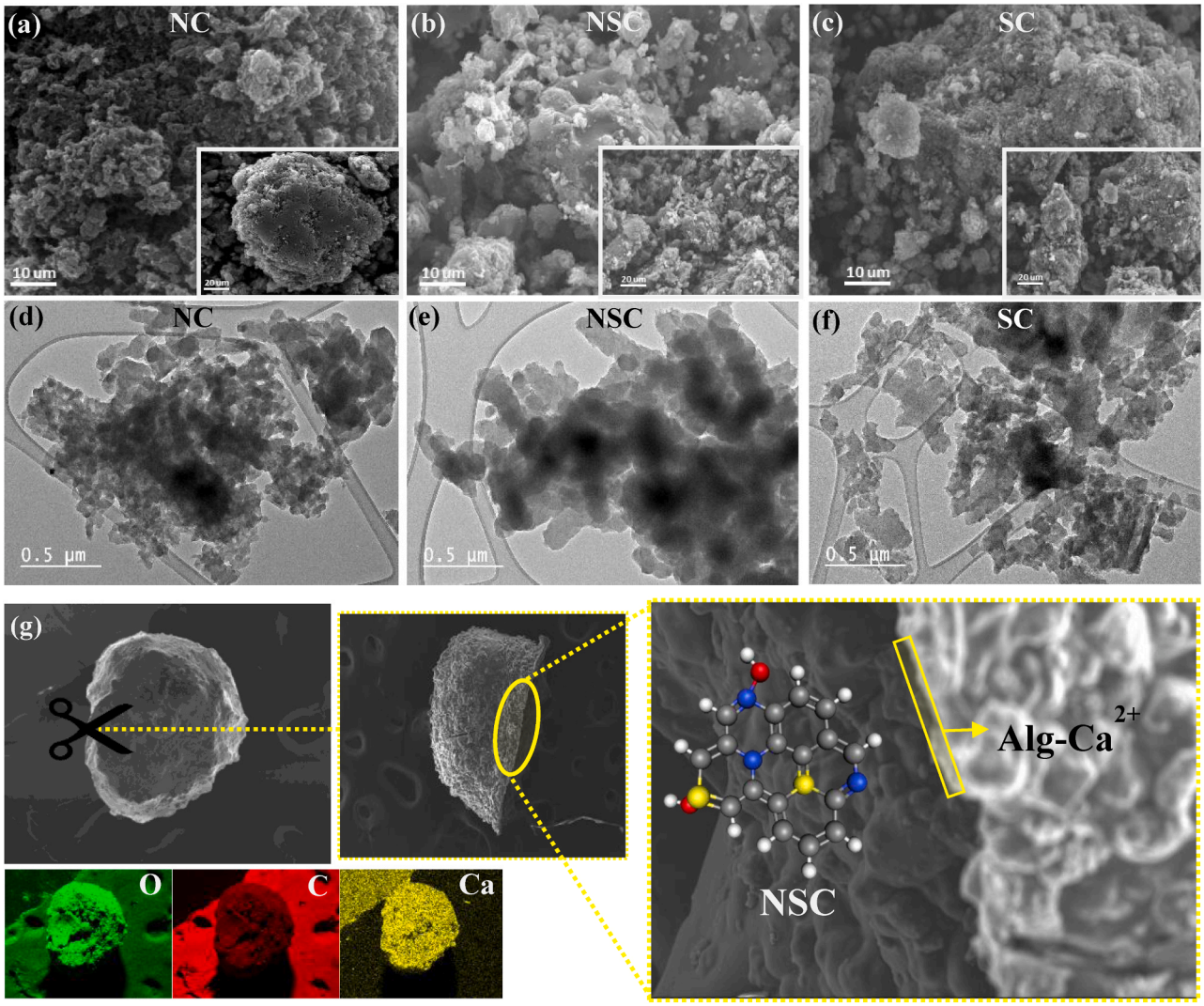

Fig. 2. SEM images of NC (a), NSC (b) and SC (c). TEM images of NC (d), NSC (e) and SC (f); SEM and mapping images of NSC@Alg (g).

summarized in Fig. 4a and b, and the corresponding reaction rate constants are gathered in Fig. 4c. Thus, the OG adsorptions on various samples were significant and reached up to about, 49% in the SC system, 46% for NSC, and 44% for NC, with adsorbed amounts of about 119, 112 and 95 mg g^{-1} for SC, NSC and NC, respectively. as resulting from their large specific surface areas. Moreover, as can be seen in Fig. 4a, a limited OG degradation was observed in the PS system alone, suggesting that the PS could not promise significant removal of OG without its activation by the carbocatalyst. The OG removal with the two mono-doped carbocatalysts, increases to 80% and reaches 100%, within 24 min, yielding reaction rate constants of 0.076 and 0.131 min^{-1}, respectively, in the SC/PS and the NC/PS systems. However, the N and S co-doped carbon (NSC) was found to have the highest catalytic activity with a total degradation in the first 15 min yielding the highest reaction rate constant of 0.338 min^{-1}. Likewise, the NSC/PS system also shows the highest degradation for BPA and RhB pollutants (Fig. 4d and e), when compared to the NC/PS and the SC/PS systems. In the case of the RhB degradation (Fig. 4e), it can be clearly seen in the figure that the reaction rate constant has significantly increased for NSC (0.201 min^{-1}) than NC (0.089 min^{-1}) and SC (0.058 min^{-1}). Regarding the BPA degradation (Fig. 4d), the reaction rate constant was also important in the NSC/PS system (0.143 min^{-1}), in comparison to the NC (0.072 min^{-1}) and the SC (0.050 min^{-1}). Such results suggest that the introduction of the S atoms alone into the carbon structure, shows less important effect than N atoms which exhibit high catalytic activity [11,46]. However, the introduction of both N and S heteroatoms leads to the NSC carbocatalyst showing the highest catalytic activity, in comparison to the NC and SC. Such excellent catalytic effect of the NSC sample can be explained by several other factors including, its high BET surface area, and its well-defined porosity (Fig. 3 and Table 1), which allow the abundance of active sites. Other factors explaining the excellent NSC activity is due to the N, S heteroatoms amount in the carbon structure. Thus, large N, S heteroatoms amount and/or percentage are obtained in the case of conductive polymers, upon their carbonization, as shown in the XPS analysis, especially in the NSC carbocatalyst. For this reason, we have studied the relationship that may occur between the reaction rate constant, and the heteroatoms percentage, for different catalysts (Fig. 4c). Hence, as can be seen, the NSC having the largest heteroatoms percentage, in comparison to the NC and the SC samples, has also the highest OG reaction rate constant degradation. It is therefore expected that doping an appropriate amount of N and S, at the same time in the structure, can create a synergistic effect in enhancing persulfate activation and ROS generations. However, the generated ROS in the carbocatalyst/PS systems normally exhibit high oxidation potential, leading to insufficient mineralization of the total organic carbons (Text S1. and Fig. S3).

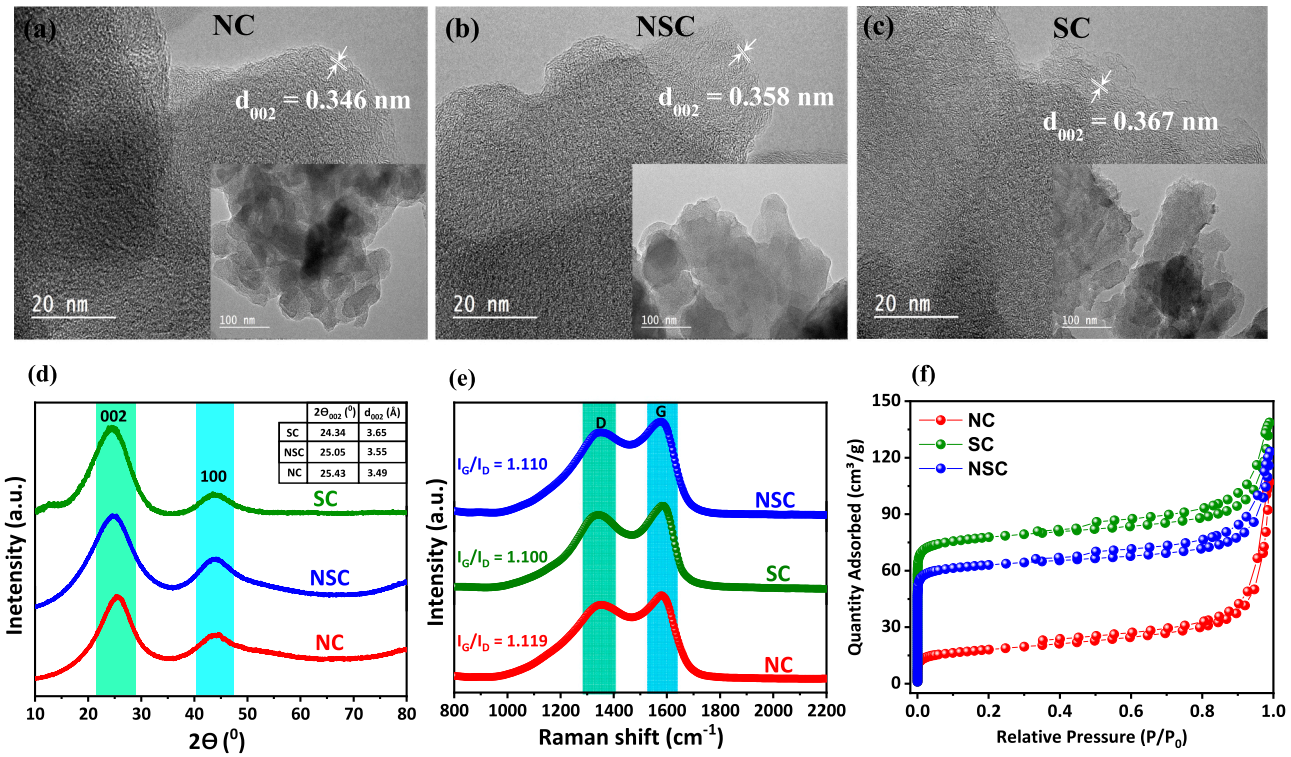

	2Θ002 (0)	d002 (Å)
SC	24.34	3.65
NSC	25.05	3.55
NC	25.43	3.49

Fig. 3. High-resolution TEM images of (a) NC, (b) NSC and (c) SC, with their average lattice fringe spacings indicated in the figures. XRD (d) and Raman (e) spectra, Nitrogen adsorption and desorption isotherms (f), of various carbocatalysts.

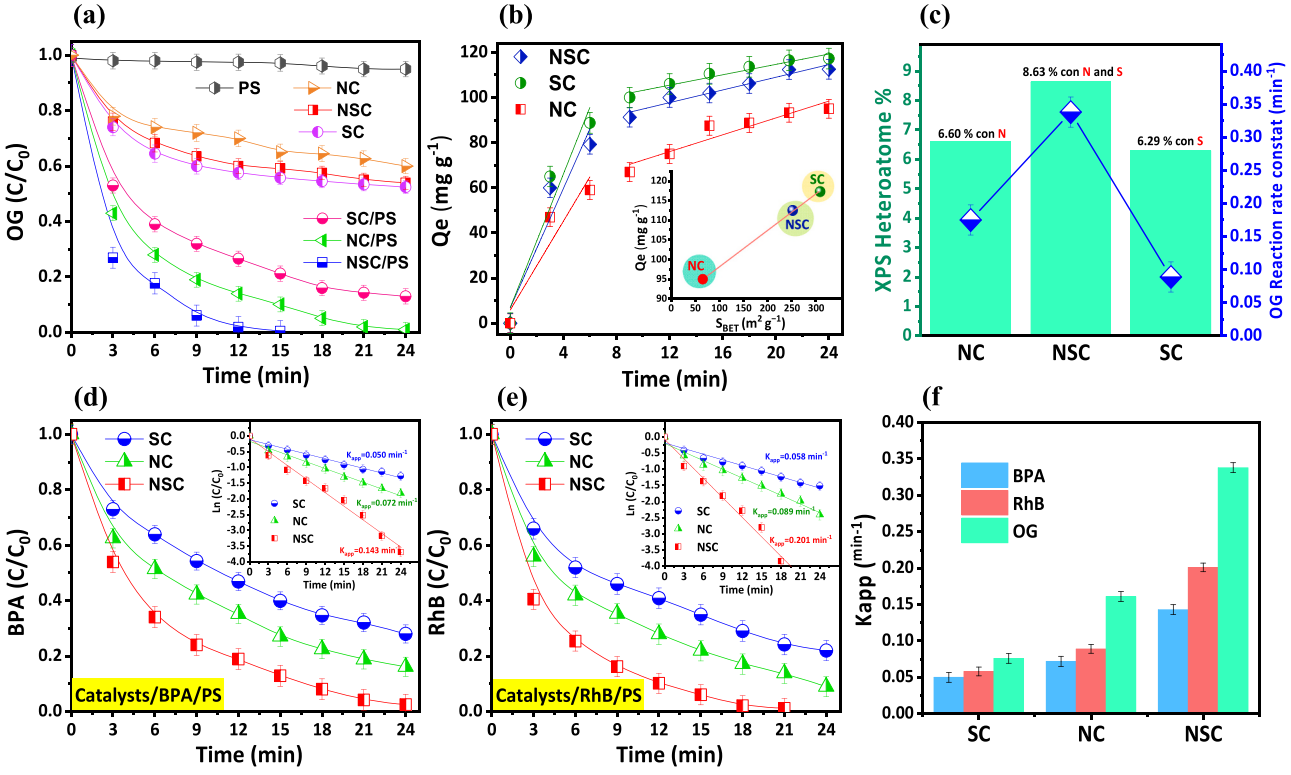

Fig. 4. (a) Degradation profiles of OG, (b) Adsorption of OG, (c) The relation between XPS heteroatoms concentration and the reaction rate constants, (d) Degradation profiles of BPA, (e) Degradation profiles of RhB, and (f) Reaction rate constants of different carbo-catalysts. Reaction conditions: [Catalyst] = 0.2 g L^{-1}, [OG] = 50 mg L^{-1}, [PS] = 4 mM; [BPA] = 10 mg L^{-1}; [RhB] = 20 mg L^{-1}.

3.3. ROS analyses and synergistic mechanism

The radical quenching tests were carried out in order to investigate the main ROS generated during the PS activation on different systems studied. Thus, ethanol (EtOH) and tert-butanol (TBA) were used as selective free radical scavengers, to distinguish the contribution of both radicals $SO_4^{\bullet-}$ and $OH^{\bullet}$ in the NSC/PS, NC/PS and SC/PS systems [10,11,47,48]. Hence, it was shown that EtOH can scavenge both radical $OH^{\bullet}$ ($k = 1.8–2.8$) $\times 10^9\ M^{-1}\ s^{-1}$) and $SO_4^{\bullet-}$ ($k = 1.6–6.2$) $\times 10^7\ M^{-1}\ s^{-1}$) [10,11,49], while the TBA react only with $OH^{\bullet}$($k = 3.8–7.6 \times 10^8\ M^{-1}\ s^{-1}$) [25,48,50,51]. Fig. 5a-d show that the catalytic efficiencies of the different systems are slightly slowed down upon the addition of EtOH and TBA, showing hence radical deactivation effects. Further, the addition of EtOH and TBA scavengers, affects little the reaction rate constants, which are weakly decreased, indicating that $SO_4^{\bullet-}$ and $OH^{\bullet}$ radicals are not the dominated generated ROS in these catalytic systems. It has been reported that doping and co-doping with heteroatoms in the carbon structure could increase the PS adsorption energy on the catalysts surface, thus transforming the adsorbed activated complexes by a non-radical process. In addition to $SO_4^{\bullet-}$ and $OH^{\bullet}$ radicals, the superoxide intermediate ($O_2^{\bullet-}$) is also an important reactive species in the radical oxidation reaction. The $O_2^{\bullet-}$scavenging experiments were realized by using p-benzoquinone (p-BQ) as a selective quencher with high reaction rate toward $O_2^{\bullet-}$($k = 9 \times 10^8\ M^{-1}\ S^{-1}$) [25,50,51]. Figs. 5b and d show that the catalytic activities of NSC are slightly decreased after the addition of p-BQ, and the reaction rate constant is weakly weakened from 0.338 to 0.277 min^{-1}, suggesting that $O_2^{\bullet-}$is not the dominant ROS in NSC/PS system. It has been reported that the $O_2^{\bullet-}$ radical, as an intermediate, can transform easily into $^1O_2$, in the catalytic systems [50–54]. In addition, the singlet oxygen $^1O_2$ plays an important role in the non-radical oxidation pathway. Thus, in order to confirm the generation of the singlet oxygen $^1O_2$, quenching experiments were realized by using L-Histidine is an excellent scavenger for $^1O_2$ [25,55]. As shown in Fig. 5a–d the catalytic activities of NSC, NC and SC, were significantly decreased upon the addition of L-Histidine, and the reaction rate constants decreased from 0.338 to 0.051 min^{-1}, from 0.161 to 0.033 min^{-1} and from 0.076 to 0.025 min^{-1}, respectively, in the NSC/PS, NC/PS and SC/PS systems. The results indicated that a large amount of $^1O_2$ should be produced in the different studied systems. The scavenging experiments carried out by L-Histidine, clearly prove that $^1O_2$ plays a more important role than $SO_4^{\bullet-}$ and $OH^{\bullet}$ during the catalysis process in view of the pollutant degradation. The involvement of ROS in such degradation reaction was further checked and confirmed by electron paramagnetic resonance (EPR) by using PBN as a spin-trapping agent for $SO_4^{\bullet-}$ and $OH^{\bullet}$ [10,11], and TEMP as a spin-trapping agent for $^1O_2$ in the various catalytic reactions [48,50,56]. As shown in Fig. 5e and f, straight line was observed in the presence of either PBN or TEMP agent, when the PS alone was involved in the various catalytic processes, indicating that no radical was generated. In comparison, evident characteristic peaks appeared in the EPR spectra when the PS activation was achieved in the presence of various catalysts. Thus, the EPR spectra (Fig. 5e) clearly show the characteristic signals for PBN-$SO_4^{\bullet-}$ and PBN-$OH^{\bullet}$ suggesting the generation of $SO_4^{\bullet-}$ and $OH^{\bullet}$ radicals in various carbocatalyst/PS systems. Furthermore, the magnitudes in the PBN-$SO_4^{\bullet-}$ and PBN-$OH^{\bullet}$ signals were higher in the NSC/PS system in comparison to PBN-X signals of the NC/PS and SC/PS systems, showing hence the abundant generation of radicals in the NSC/PS system. More importantly, a strong characteristic triplet signal was systematically observed when TEM was involved as a spin agent (Fig. 5f), confirming further the $^1O_2$ generation in the various oxidation systems studied. Note also that the intensity of the TEMP-$^1O_2$ peaks in the NSC/PS catalytic system was greater and significant when compared to the NC/PS and SC/PS systems, indicating that co-doping of N and S creates a synergistic effect, which enhances the persulfate activation and facilitates the production of the reactive species $^1O_2$. The overall EPR data are consistent with the various radical deactivation tests. Therefore, the non-radical pathway expressed by the involvement of $^1O_2$ has been proposed as a dominant catalytic reaction mechanism in the systems studied, whereas the radical pathway involving the $SO_4^{\bullet-}$ and $OH^{\bullet}$ radicals played a minor role.

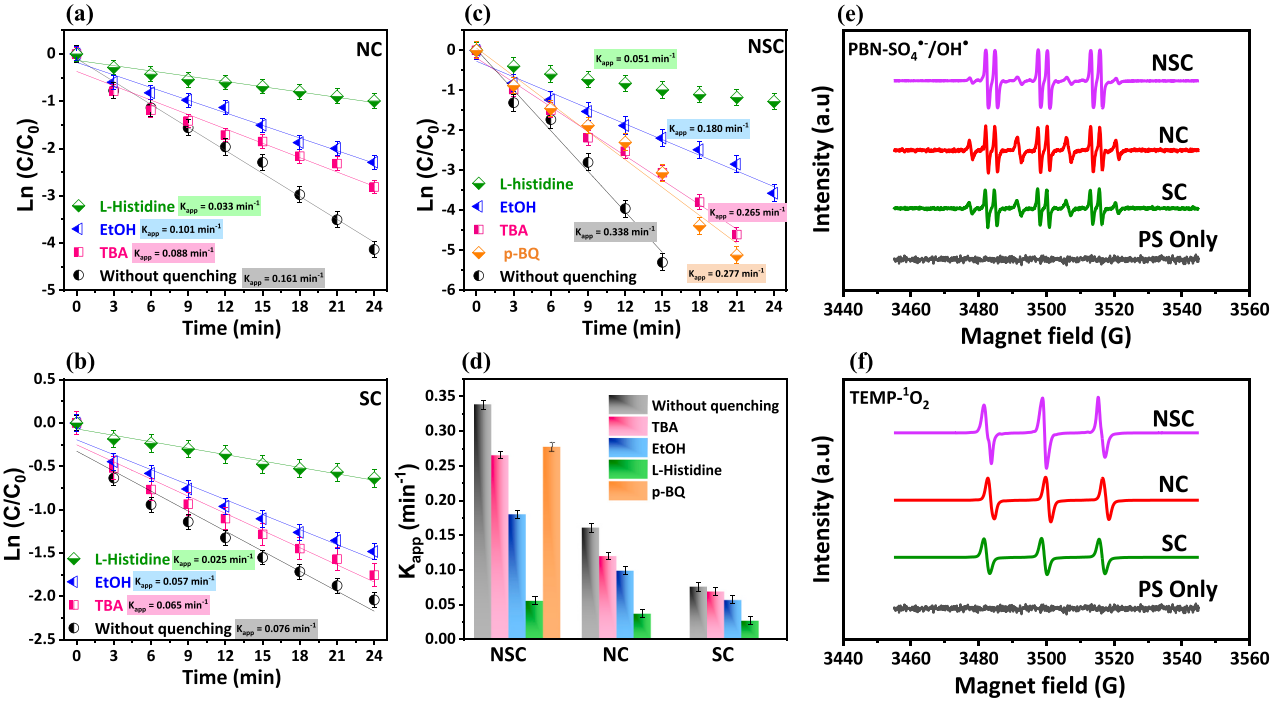

Fig. 5. Pseudo-first order kinetics of different scavengers, on the OG degradation in (a) NC/PS, (b) SC/PS, (c) NSC/PS, (d) Effects of various scavengers on the OG degradation reaction rate constants. (Experimental conditions: [Catalyst] = 0.2 g L^{-1}, [OG] =50 mg L^{-1}, [PS] = 4 mM, [EtOH] = [TBA] = 1 M, [L-Histidine] =50 Mm, [p-BQ] =50 mM) and (e, f) EPR spectra by using PBN and TEMP as spin-trapping agents).

Generally, in the SR-AOPs, the use of N and S heteroatoms doped carbon materials can improve the catalytic activity towards the PS activation. Since the carbon atom electronegativity is very low, as compared to nitrogen, and almost the same for Sulfur, the reassembly of these atoms will result, at molecular level, in various chemical structures and electronic charges distributions [24,29,31,50,56]. Such distribution in the electronic charges will, in turn, lead to the apparition of active sites on the surface material, allowing the $S_2O_8^{2-}$ ions adsorption, facilitating the cleavage of O-O bond, and generating the ROS [31,50,56]. Note that the graphitic N is the main active for the non-radical PS activation. Furthermore, the electron-rich N groups (pyrrolic N and pyridinic N) present on the carbocatalysts surface, could also participate to the cleavage of the O-O bond, producing hence $SO_4^{\bullet-}$ species via the radical pathway [33,34]. However, in the case of a catalyst structure consisting basically of carbon and sulfur atoms, the O-O bond cleavage of the PS, will be initiate by thiophenic S (-C-S-C-) active sites rich in electron [14]. In summary, the graphitic N and thiophenic S heteroatoms play critical roles in the PS activation process [24,25,56]. However, the mechanism of the PS activation by N and S heteroatoms co-doped carbon is not yet well known, for this we tried to propose in the present work a possible mechanism of the PS activation (Scheme 2). As it was already shown in the present work, the sulfur, when compared to nitrogen atoms, create more structural defects in the carbon matrix, therefore a question can then be asked: Is it possible that proper doping of N and S could create a synergistic defect-charge effect, and improve the catalytic persulfate activation? This is the question to which we were trying to answer in the present work. The overall data have shown that the doping by S atoms makes the catalyst surface less graphitic while the doping by N atoms leads to a larger negative charge distribution. However, the co-doping by S and N atoms (NSC) gives at the same time: an acceptable electronic distribution to promote the adsorption process with optimal structural defects and creates a synergistic effect between the graphitic N and the thiophenic S with the redistribution of spin and charge density, and an increase in active sites on the catalyst surface. Such catalyst surface due to the N, S co-doping facilitates the electrons acceptance from the PS ion ($S_2O_8^{2-}$), reinforcing hence the persulfate activation and generating the $^1O_2$ which could effectively degrade the organic molecules [29,31,56]. The $^1O_2$ generation results from both, the synergetic effect of N and S dopants reinforcing the electrons extraction from the adjacent positive carbon atom which is linked with the $S_2O_8^{2-}$ to produce $^1O_2$ (Eqs. (1) and (2)), and the generation, upon the PS activation, of superoxide radicals $O_2^{\bullet-}$ as precursor of the singlet oxygen $^1O_2$ (Eq. (3)) [50,52]. On the other hand, the electron transfers from N and S sites to PS led to the generation of $SO_4^{\bullet-}$ which could further yield $OH^{\bullet}$ (Eqs. (4) and (5)). The co-doping procedure was found to be an appropriate choice and exhibiting a huge effect and is concluded that a new generation pathway of ROS by synergistic effect between the doping elements.

$$NSC+SO_3^-\text{-}O\text{-}O\text{-}SO_3^- \rightarrow NSC|SO_3^-\text{-}O\text{-}O\text{-}SO_3^- \quad (1)$$

$$NSC|SO_3^-\text{-}O\text{-}O\text{-}SO_3^- + 2H_2O \rightarrow NSC|{}^1O_2 + 4H^+ + 2SO_4^{2-} \quad (2)$$

$$2\,O_2^{\bullet-} + 2H_2O \rightarrow {}^1O_2 + H_2O_2 + 2OH^- \quad (3)$$

$$NSC|SO_3^-\text{-}O\text{-}O\text{-}SO_3^- \rightarrow NSC + SO_4^{\bullet-} + SO_4^{2-} \quad (4)$$

$$SO_4^{\bullet-} + H_2O \rightarrow OH^{\bullet} + SO_4^{2-} + H^+ \quad (5)$$

3.4. Separation, stability and reusability

It is well known that the study of the stability, the reusability, and the separation during the reuse of the catalysts, is very important in practical applications. These problems arise mostly when the carbocatalysts are used in the PS activation. The researchers aiming to develop metal-free catalysts, with separable and recyclable properties, are very important in the practical side. In our study we have prepared metal-free carbocatalysts in the form of hydrogel beads from alginate biopolymers (NSC@Alginate), which are separable and stable during their reuse. To check the durability for NSC and NSC@Alginate samples, the reuse tests were carried out and are presented in the Fig. 6a and b. As can be observed in this figure, after five cycles of reuse of NSC, the catalytic efficiency decreases significantly from 100% to 64%, in addition, after each cycle, the subsequent filtration process was accompanied with a mass loss. The decrease in the catalytic efficiency observed for the NSC sample during its reuse, is due to surface structural changes resulting from the active sites loss (S thiophenic and N graphitic), and the pore filling by the intermediate's adsorption. Regarding the NSC@Alginate beads, no decrease was observed after 5 cycles of use, showing high stability. Moreover, the hydrogel beads were found to be easily recovered from solutions and reused with no loss in their mass due to their large particle size. It is obvious that the increase in the stability after the NSC transformation into hydrogel beads is due to the decrease of the active sites leaching (S thiophenic and N graphitic) after the coating of the NSC with the alginate and calcium ions complex. Despite the increase in the

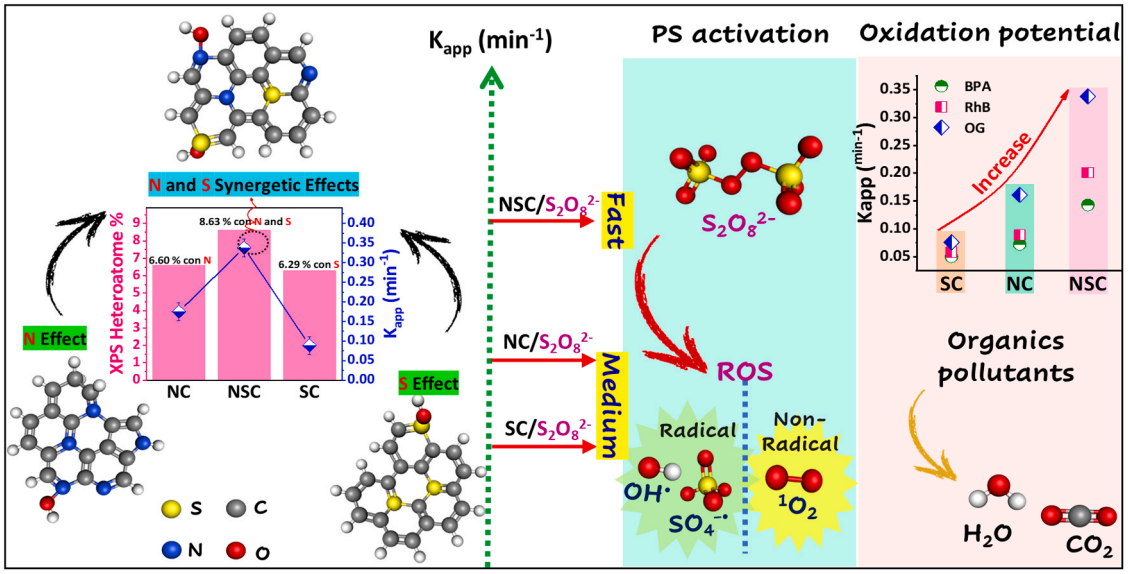

Scheme 2. Proposed mechanism of PS activation in NSC, NC and SC catalysts.

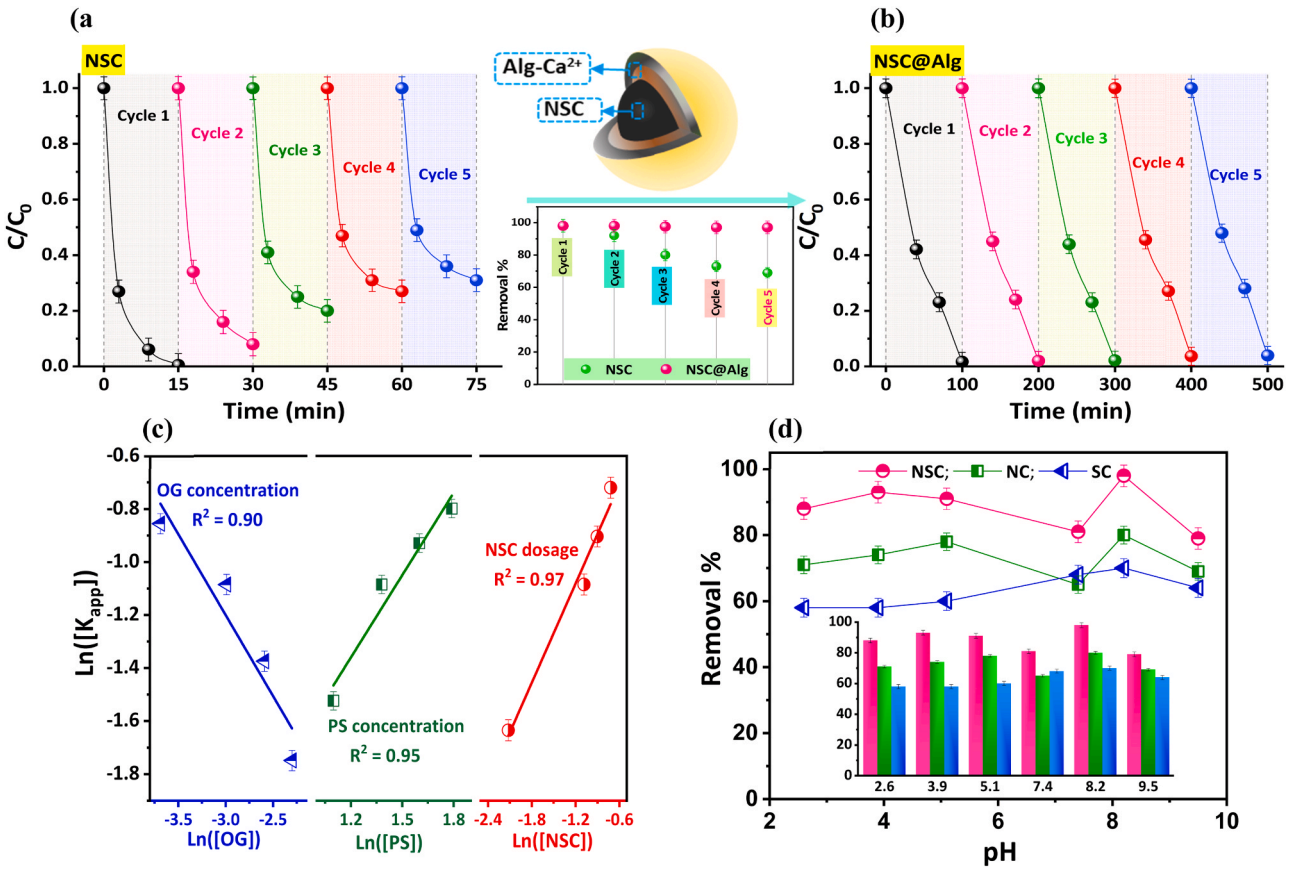

Fig. 6. Stability and reusability of NSC (a), NSC@Alginate (b); Effect of initial pH solution (d)([Catalyst] = 0.2 g L^{-1}, [OG] =50 mg L^{-1}, [PS] = 4 mM). Linear correlations between catalyst dose, PS concentration, OG concentration and kapp in NSC/PS (c): ([catalyst] = 0.1, 0.2, 0.3, 0.4 g L^{-1}, [OG] = 25, 50, 75, 100 mg L^{-1}, [PS] = 3, 4, 5, 6 mM).

catalytic reaction time observed for the NSC@Alginate hydrogel beads, we have confirmed its stability, reusability, easy synthesis environmentally friendly aspect, indicating therefore that the hydrogel beads catalyst is suitable for industrial applications.

3.5. *Factors affecting the OG degradation*

To further determine the keys factors affecting the OG degradation, we have studied the effects of various experimental conditions such as the dosage of the carbocatalyst, the dosage of PS, the concentration of pollutants and the initial solution pH, in addition, the effect of the water matrix.

The effects of catalyst dose, PS concentration and OG concentration on the catalytic process were investigated (Fig. 6c). Linear relationships between ln (Kapp) and (ln([NSC], ln([PS]) and ln([OG])) have been established. Fig. 6c shows that the pollutant degradation reaction rate constant (kapp) is strongly related to the experimental conditions. Thus, the Kapp increases when the NSC dose increases from 0.1 g L^{-1} to 0.4 g L^{-1}. In summary, the high performance of the carbocatalyst, is attributed to the creation of more active sites that results from the synergistic effects occurring on the NSC surface, increasing hence the electrons transfer from the catalyst to the PS, and generating more reactive species, especially $^1O_2$. Likewise, the effect of the PS concentration is positive when it increases from 2 to 8 mM, the reaction kinetics become faster due to sufficient electrostatic interactions occurring between the nucleophile $S_2O_8^{2-}$ and the electrophilic NSC surface sites indicating a significant release of ROS. However, a negative linear correlation was observed between Kapp and OG concentration which could be due to the occurrence of insufficient NSC active sites upon the OG concentration increase. The initial solution pH is an important factor affecting the degradation of organic pollutants. The degradation efficiencies by the different systems were assessed by varying the initial pH value from 2.6 to 9.5. The different results are gathered in Fig. 6d, and show that the catalytic efficiency of the NSC, NC and SC are better in alkaline and acidic environments. In short, the carbocatalysts can be applied for the PS activation in a wide pH range. To further investigate the feasibility of NSC in the environment, the NSC effect on the OG degradation in tap water (TW) matrix was investigated. Fig. S4 shows that the removal of OG was slightly depleted by 100% and 78% in 15 min. This could be due to the high conductivity, and the chloride ions present in TW inhibit the generation of ROS. This indicates that the catalysts/PS systems are also effective in removing OG from the actual water samples.

4. Conclusion

In this work, N or S mono-doped, and N, S co-doped carbon carbocatalysts, were synthesized by one-pot process from direct carbonization of conjugated polymers for organic pollutants degradation. Experimental and characterization insights were realized to establish an existing relationship between the PS activation dependent on the carbocatalysts structure and the catalytic oxidation reaction. The catalytic reaction rate was found to be strongest in the case of N, S co-doped carbon as compared to individual N or S doped material. The highly catalytic activity of the NSC catalyst was due to the synergistic effect occurring between N and S heteroatoms dopants, especially, the N graphitic and S thiophenic. Further, the scavenging experiments have shown that the non-radical pathways dominate the catalytic reaction rather than the processes generating the radical species such as $SO_4^{\bullet-}$, $OH^{\bullet}$ and $O_2^{\bullet-}$. Moreover, the singlet oxygen was the major reactive

oxygen species involved in the pollutant degradation reaction, as shown from the EPR analyzes. The formulation of the carbocatalysts with alginate aqueous solution led to the formation of separable NSC@Alginate hydrogel beads having higher catalytic activity and excellent chemical stability for organic pollutants degradation. In overall, the design of N, S co-doped carbon materials, leads to scalable carbocatalysts, highly performants, and having improved activity toward the wastewater treatment.

CRediT authorship contribution statement

Abdellah Ait El Fakir: Writing – original draft, Conceptualization, Methodology, Data curation, Writing – review & editing. **Zakaria Anfar:** Methodology, Conceptualization, Data curation, Writing – review & editing. **Mohamed Enneiymy:** Data curation, Writing – review & editing. **Amane Jada:** Project administration, Supervision, Validation, Writing – review & editing. **Noureddine El Alem:** Project administration, Supervision, Writing – review & editing.

Declaration of Competing Interest

The authors declare that they have no known competing financial interests or personal relationships that could have appeared to influence the work reported in this paper.

Acknowledgments

This work was supported by Franco-Moroccan Cooperation Framework under both grant research projects APUR 2019 and CEDocs 2018 managed by Laboratory of Materials & Environment (LME), Ibn Zohr University, Agadir – Morocco and the Institute of Materials Science of Mulhouse (IS2M), Haute Alsace University, Mulhouse – France. We thank, VAULOT Cyril (IS2M), VIDAL Loïc (IS2M), FIOUX Philippe (IS2M), MORLET - SAVARY Fabrice (IS2M) and GREE Simon (IS2M) for the analyses of samples by BET, TEM, XPS, EPR and Raman, respectively.

Appendix A. Supporting information

Supplementary data associated with this article can be found in the online version at doi:10.1016/j.apcatb.2021.120732.

References

[1] Z.-H. Xie, H.-Y. Zhou, C.-S. He, Z.-C. Pan, G. Yao, B. Lai, Synthesis, application and catalytic performance of layered double hydroxide based catalysts in advanced oxidation processes for wastewater decontamination: a review, Chem. Eng. J. 414 (2021), 128713, https://doi.org/10.1016/j.cej.2021.128713.

[2] X. Duan, H. Sun, S. Wang, Metal-free carbocatalysis in advanced oxidation reactions, Acc. Chem. Res. 51 (2018) 678–687, https://doi.org/10.1021/acs.accounts.7b00535.

[3] J. Yu, H. Feng, L. Tang, Y. Pang, G. Zeng, Y. Lu, H. Dong, J. Wang, Y. Liu, C. Feng, J. Wang, B. Peng, S. Ye, NaGdF4:Yb/Er nanoparticles of different sizes for tracking mesenchymal stem cells and their effects on cell differentiation, Mater. Sci. Eng. C Mater. Biol. Appl. 111 (2020), 110827, https://doi.org/10.1016/j.pmatsci.2020.100654.

[4] M.-P. Zhu, J.-C.E. Yang, X. Duan, S. Wang, D.D. Sun, B. Yuan, M.-L. Fu, Engineered Co2AlO4/CoAl2O4@Al2O3 monolithic catalysts for peroxymonosulfate activation: Co3+/Co2+ and ODefect/OLattice ratios dependence and mechanism, Chem. Eng. J. 409 (2021), 128162, https://doi.org/10.1016/j.cej.2020.128162.

[5] S. Liu, B. Jing, C. Nie, Z. Ao, X. Duan, B. Lai, Y. Shao, S. Wang, T. An, Piezoelectric activation of peroxymonosulfate by MoS 2 nanoflowers for the enhanced degradation of aqueous organic pollutants, Environ. Sci. Nano (2021), https://doi.org/10.1039/D0EN01237H.

[6] P. Zhou, F. Cheng, G. Nie, Y. Yang, K. Hu, X. Duan, Y. Zhang, S. Wang, Boron carbide boosted Fenton-like oxidation: a novel Fe(III)/Fe(II) circulation, Green, Energy Environ. 5 (2020) 414–422, https://doi.org/10.1016/j.gee.2020.09.007.

[7] T. Olmez-Hanci, I. Arslan-Alaton, S. Gurmen, I. Gafarli, S. Khoei, S. Safaltin, D. Yesiltepe Ozcelik, Oxidative degradation of Bisphenol A by carbocatalytic activation of persulfate and peroxymonosulfate with reduced graphene oxide, J. Hazard. Mater. 360 (2018) 141–149, https://doi.org/10.1016/j.jhazmat.2018.07.098.

[8] X. Duan, Z. Ao, H. Sun, S. Indrawirawan, Y. Wang, J. Kang, F. Liang, Z.H. Zhu, S. Wang, Nitrogen-doped graphene for generation and evolution of reactive radicals by metal-free catalysis, ACS Appl. Mater. Interfaces 7 (2015) 4169–4178, https://doi.org/10.1021/am508416n.

[9] J. Wang, Q. Gong, J. Ali, M. Shen, J. Cai, X. Zhou, Z. Liao, S. Wang, Z. Chen, pH-dependent transformation products and residual toxicity evaluation of sulfamethoxazole degradation through non-radical oxygen species involved process, Chem. Eng. J. 390 (2020), 124512, https://doi.org/10.1016/j.cej.2020.124512.

[10] A. Ait El Fakir, Z. Anfar, A. Amedlous, M. Zbair, Z. Hafidi, M. El Achouri, A. Jada, N. El Alem, Engineering of new hydrogel beads based conducting polymers: metal-free catalysis for highly organic pollutants degradation, Appl. Catal. B: Environ. 286 (2021), 119948, https://doi.org/10.1016/j.apcatb.2021.119948.

[11] Z. Anfar, A.A. El Fakir, M. Zbair, Z. Hafidi, A. Amedlous, M. Majdoub, S. Farsad, A. Amjlef, A. Jada, N. El Alem, New functionalization approach synthesis of Sulfur doped, Nitrogen doped and Co-doped porous carbon: superior metal-free Carbocatalyst for the catalytic oxidation of aqueous organics pollutants, Chem. Eng. J. 405 (2021), 126660, https://doi.org/10.1016/j.cej.2020.126660.

[12] S. Ye, G. Zeng, X. Tan, H. Wu, J. Liang, B. Song, N. Tang, P. Zhang, Y. Yang, Q. Chen, X. Li, Nitrogen-doped biochar fiber with graphitization from Boehmeria nivea for promoted peroxymonosulfate activation and non-radical degradation pathways with enhancing electron transfer, Appl. Catal. B: Environ. 269 (2020), 118850, https://doi.org/10.1016/j.apcatb.2020.118850.

[13] P. Sun, H. Liu, M. Feng, Z. Zhai, Y. Fang, X. Zhang, V.K. Sharma, Strategic combination of N-doped graphene and g-C3N4: efficient catalytic peroxymonosulfate-based oxidation of organic pollutants by non-radical-dominated processes, Appl. Catal. B: Environ. 272 (2020), 119005, https://doi.org/10.1016/j.apcatb.2020.119005.

[14] Y. Guo, Z. Zeng, Y. Zhu, Z. Huang, Y. Cui, J. Yang, Catalytic oxidation of aqueous organic contaminants by persulfate activated with sulfur-doped hierarchically porous carbon derived from thiophene, Appl. Catal. B Environ. 220 (2018) 635–644, https://doi.org/10.1016/j.apcatb.2017.08.073.

[15] A. Ait El Fakir, Z. Anfar, M. Benafqir, A. Jada, N. El Alem, Polyaniline coated hematite sand supported on graphene oxide (HS@PANI-GO) as a new magnetic material for advanced catalytic oxidation based on sulfate radicals: optimization using response surface methodology, J. Chem. Technol. Biotechnol. 94 (2019) 2609–2620, https://doi.org/10.1002/jctb.6070.

[16] A. Ait El Fakir, Z. Anfar, A. Amedlous, A. Amjlef, S. Farsad, A. Jada, N. El Alem, Synergistic effect for efficient catalytic persulfate activation in conducting polymers-hematite sand composites: enhancement of chemical stability, Appl. Catal. A: Gen. 623 (2021), 118246, https://doi.org/10.1016/j.apcata.2021.118246.

[17] Z. Anfar, A. Amedlous, M. Majdoub, A.A. El Fakir, M. Zbair, H. Ait Ahsaine, A. Jada, N. El Alem, New amino group functionalized porous carbon for strong chelation ability towards toxic heavy metals, RSC Adv. 10 (2020) 31087–31100, https://doi.org/10.1039/D0RA05220E.

[18] J. Wang, M. Shen, Q. Gong, X. Wang, J. Cai, S. Wang, Z. Chen, One-step preparation of ZVI-sludge derived biochar without external source of iron and its application on persulfate activation, Sci. Total Environ. 714 (2020), 136728, https://doi.org/10.1016/j.scitotenv.2020.136728.

[19] M. Pedrosa, G. Drazic, P.B. Tavares, J.L. Figueiredo, A.M.T. Silva, Metal-free graphene-based catalytic membrane for degradation of organic contaminants by persulfate activation, Chem. Eng. J. 369 (2019) 223–232, https://doi.org/10.1016/j.cej.2019.02.211.

[20] Y. Wang, H. Wang, J. Li, X. Zhao, Silver nanoparticles decorated magnetic polymer composites (Fe3O4@PS@Ag) as highly efficient reusable catalyst for the degradation of 4-nitrophenol and organic dyes, J. Environ. Manag. 278 (2021), 111473, https://doi.org/10.1016/j.apcatb.2020.118981.

[21] X. Cheng, H. Guo, W. Li, B. Yang, J. Wang, Y. Zhang, E. Du, Metal-free carbocatalysis for persulfate activation toward nonradical oxidation: enhanced singlet oxygen generation based on active sites and electronic property, Chem. Eng. J. 396 (2020), 125107, https://doi.org/10.1016/j.cej.2020.125107.

[22] Y. Guo, Z. Zeng, Y. Li, Z. Huang, Y. Cui, In-situ sulfur-doped carbon as a metal-free catalyst for persulfate activated oxidation of aqueous organics, Catal. Today 307 (2018) 12–19, https://doi.org/10.1016/j.cattod.2017.05.080.

[23] H. Liu, P. Sun, M. Feng, H. Liu, S. Yang, L. Wang, Z. Wang, Nitrogen and sulfur co-doped CNT-COOH as an efficient metal-free catalyst for the degradation of UV filter BP-4 based on sulfate radicals, Appl. Catal. B Environ. 187 (2016) 1–10, https://doi.org/10.1016/j.apcatb.2016.01.036.

[24] P. Sun, H. Liu, M. Feng, L. Guo, Z. Zhai, Y. Fang, X. Zhang, V.K. Sharma, Nitrogen-sulfur co-doped industrial graphene as an efficient peroxymonosulfate activator: singlet oxygen-dominated catalytic degradation of organic contaminants, Appl. Catal. B Environ. 251 (2019) 335–345, https://doi.org/10.1016/j.apcatb.2019.03.085.

[25] K. Zhu, Y. Shen, J. Hou, J. Gao, D. He, J. Huang, H. He, L. Lei, W. Chen, One-step synthesis of nitrogen and sulfur co-doped mesoporous graphite-like carbon nanosheets as a bifunctional material for tetracycline removal via adsorption and catalytic degradation processes: Performance and mechanism, Chem. Eng. J. 412 (2021), 128521, https://doi.org/10.1016/j.cej.2021.128521.

[26] K.-Y.A. Lin, M.-T. Yang, Z.-Y. Zhang, T. Wi-Afedzi, Y.-F. Lin, Prussian Blue analogue supported on sulfur-doped carbon nitride as an enhanced heterogeneous catalyst for activating peroxymonosulfate, J. Colloid Interface Sci. 529 (2018) 161–170, https://doi.org/10.1016/j.jcis.2018.05.039.

[27] K.-Y.A. Lin, Z.-Y. Zhang, Degradation of Bisphenol A using peroxymonosulfate activated by one-step prepared sulfur-doped carbon nitride as a metal-free heterogeneous catalyst, Chem. Eng. J. 313 (2017) 1320–1327, https://doi.org/10.1016/j.cej.2016.11.025.

[28] L. Tang, Y. Liu, J. Wang, G. Zeng, Y. Deng, H. Dong, H. Feng, J. Wang, B. Peng, Enhanced activation process of persulfate by mesoporous carbon for degradation of aqueous organic pollutants: electron transfer mechanism, Appl. Catal. B Environ. 231 (2018) 1–10, https://doi.org/10.1016/j.apcatb.2018.02.059.
[29] X. Huo, P. Zhou, J. Zhang, Y. Liu, X. Cheng, Y. Liu, W. Li, Y. Zhang, N, S-Doped porous carbons for persulfate activation to remove tetracycline: nonradical mechanism, J. Hazard. Mater. 391 (2020), 122055, https://doi.org/10.1016/j.jhazmat.2020.122055.
[30] X. Duan, K. O'Donnell, H. Sun, Y. Wang, S. Wang, Sulfur and nitrogen Co-doped graphene for metal-free catalytic oxidation reactions, Small 11 (2015) 3036–3044, https://doi.org/10.1002/smll.201403715.
[31] W. Tian, H. Zhang, X. Duan, H. Sun, M.O. Tade, H.M. Ang, S. Wang, Nitrogen- and sulfur-codoped hierarchically porous carbon for adsorptive and oxidative removal of pharmaceutical contaminants, ACS Appl. Mater. Interfaces 8 (2016) 7184–7193, https://doi.org/10.1021/acsami.6b01748.
[32] H. Luo, X. Zhou, Q. Chen, J. Zhou, Removal of 2,4-dichlorophenoxyacetic acid by the boron-nitrogen co-doped carbon nanotubes: insights into peroxymonosulfate adsorption and activation, Sep. Purif. Technol. 259 (2021), 118196, https://doi.org/10.1016/j.seppur.2020.118196.
[33] Z. Wang, L. Huang, Y. Wang, X. Chen, H. Ren, Activation of peroxymonosulfate using metal-free in situ N-doped carbonized polypyrrole: a non-radical process, Environ. Res. 193 (2021), 110537, https://doi.org/10.1016/j.envres.2020.110537.
[34] S. Liu, Z. Zhang, F. Huang, Y. Liu, L. Feng, J. Jiang, L. Zhang, F. Qi, C. Liu, Carbonized polyaniline activated peroxymonosulfate (PMS) for phenol degradation: role of PMS adsorption and singlet oxygen generation, Appl. Catal. B: Environ. 286 (2021), 119921, https://doi.org/10.1016/j.apcatb.2021.119921.
[35] E. Frackowiak, V. Khomenko, K. Jurewicz, K. Lota, F. Béguin, Supercapacitors based on conducting polymers/nanotubes composites, J. Power Sources 153 (2006) 413–418, https://doi.org/10.1016/j.jpowsour.2005.05.030.
[36] Y. Ren, Z. Lin, X. Mao, W. Tian, T. Van Voorhis, T.A. Hatton, Superhydrophobic, surfactant-doped, conducting polymers for electrochemically reversible adsorption of organic contaminants, Adv. Funct. Mater. 28 (2018), 1801466, https://doi.org/10.1002/adfm.201801466.
[37] S. Ramanavicius, A. Ramanavicius, Conducting polymers in the design of biosensors and biofuel cells, Polymers (Basel) 13 (2020) 49, https://doi.org/10.3390/polym13010049.
[38] L. Sun, H. Zhou, L. Li, Y. Yao, H. Qu, C. Zhang, S. Liu, Y. Zhou, Double soft-template synthesis of nitrogen/sulfur-codoped hierarchically porous carbon materials derived from protic ionic liquid for supercapacitor, ACS Appl. Mater. Interfaces 9 (2017) 26088–26095, https://doi.org/10.1021/acsami.7b07877.
[39] Y. Li, G. Wang, T. Wei, Z. Fan, P. Yan, Nitrogen and sulfur co-doped porous carbon nanosheets derived from willow catkin for supercapacitors, Nano Energy 19 (2016) 165–175, https://doi.org/10.1016/j.nanoen.2015.10.038.
[40] Y. Su, Z. Yao, F. Zhang, H. Wang, Z. Mics, E. Cánovas, M. Bonn, X. Zhuang, X. Feng, Sulfur-enriched conjugated polymer nanosheet derived sulfur and nitrogen Co-doped porous carbon nanosheets as electrocatalysts for oxygen reduction reaction and zinc-air battery, Adv. Funct. Mater. 26 (2016) 5893–5902, https://doi.org/10.1002/adfm.201602158.
[41] Q. Dang, X. Zhang, W. Liu, Y. Wang, G. Dou, H. Zhang, G. Zhang, Hierarchical porous N,S-codoped carbon material derived from halogenated polymer for battery applications, Nano Sel. 2 (2021) 581–590, https://doi.org/10.1002/nano.202000168.
[42] Y. Cao, L. Xiao, M.L. Sushko, W. Wang, B. Schwenzer, J. Xiao, Z. Nie, L.V. Saraf, Z. Yang, J. Liu, Sodium ion insertion in hollow carbon nanowires for battery applications, Nano Lett. 12 (2012) 3783–3787, https://doi.org/10.1021/nl3016957.
[43] J. Ding, H. Wang, Z. Li, A. Kohandehghan, K. Cui, Z. Xu, B. Zahiri, X. Tan, E. M. Lotfabad, B.C. Olsen, D. Mitlin, Carbon nanosheet frameworks derived from peat moss as high performance sodium ion battery anodes, ACS Nano 7 (2013) 11004–11015, https://doi.org/10.1021/nn404640c.
[44] J. Yang, X. Zhou, D. Wu, X. Zhao, Z. Zhou, S-doped N-rich carbon nanosheets with expanded interlayer distance as anode materials for sodium-ion batteries, Adv. Mater. 29 (2017), 1604108, https://doi.org/10.1002/adma.201604108.
[45] S. Qiu, L. Xiao, M.L. Sushko, K.S. Han, Y. Shao, M. Yan, X. Liang, L. Mai, J. Feng, Y. Cao, X. Ai, H. Yang, J. Liu, Manipulating adsorption-insertion mechanisms in nanostructured carbon materials for high-efficiency sodium ion storage, Adv. Energy Mater. 7 (2017), 1700403, https://doi.org/10.1002/aenm.201700403.
[46] D. Ding, S. Yang, X. Qian, L. Chen, T. Cai, Nitrogen-doping positively whilst sulfur-doping negatively affect the catalytic activity of biochar for the degradation of organic contaminant, Appl. Catal. B: Environ. 263 (2020), 118348, https://doi.org/10.1016/j.apcatb.2019.118348.
[47] J. Li, M. Li, H. Sun, Z. Ao, S. Wang, S. Liu, Understanding of the oxidation behavior of benzyl alcohol by peroxymonosulfate via carbon nanotubes activation, ACS Catal. 10 (2020) 3516–3525, https://doi.org/10.1021/acscatal.9b05273.
[48] W. Ren, L. Xiong, X. Yuan, Z. Yu, H. Zhang, X. Duan, S. Wang, Activation of peroxydisulfate on carbon nanotubes: electron-transfer mechanism, Environ. Sci. Technol. 53 (2019) 14595–14603, https://doi.org/10.1021/acs.est.9b05475.
[49] Z. Anfar, A. Ait El Fakir, H. Ait Ahsaine, M. Zbair, S. Farsad, F. Morlet-Savary, A. Jada, N. El Alem, Nitrogen doped graphitic porous carbon from almond shells as an efficient persulfate activator for organic compound degradation, N. J. Chem. 44 (2020) 9391–9401, https://doi.org/10.1039/D0NJ01148G.
[50] X. Li, J. Wang, X. Duan, Y. Li, X. Fan, G. Zhang, F. Zhang, W. Peng, Fine-tuning radical/nonradical pathways on graphene by porous engineering and doping strategies, ACS Catal. 11 (2021) 4848–4861, https://doi.org/10.1021/acscatal.0c05089.
[51] S. Zhu, C. Jin, X. Duan, S. Wang, S.-H. Ho, Nonradical oxidation in persulfate activation by graphene-like nanosheets (GNS): differentiating the contributions of singlet oxygen (1O2) and sorption-dependent electron transfer, Chem. Eng. J. 393 (2020), 124725, https://doi.org/10.1016/j.cej.2020.124725.
[52] Y. Nosaka, A.Y. Nosaka, Generation and detection of reactive oxygen species in photocatalysis, Chem. Rev. 117 (2017) 11302–11336, https://doi.org/10.1021/acs.chemrev.7b00161.
[53] M. Hayyan, M.A. Hashim, I.M. AlNashef, Superoxide ion: generation and chemical implications, Chem. Rev. 116 (2016) 3029–3085, https://doi.org/10.1021/acs.chemrev.5b00407.
[54] Y. Chen, X. Duan, C. Zhang, S. Wang, N. Ren, S.-H. Ho, Graphitic biochar catalysts from anaerobic digestion sludge for nonradical degradation of micropollutants and disinfection, Chem. Eng. J. 384 (2020), 123244, https://doi.org/10.1016/j.cej.2019.123244.
[55] Y. Yu, N. Li, X. Lu, B. Yan, G. Chen, Y. Wang, X. Duan, Z. Cheng, S. Wang, Co/N co-doped carbonized wood sponge with 3D porous framework for efficient peroxymonosulfate activation: performance and internal mechanism, J. Hazard. Mater. 421 (2022), 126735, https://doi.org/10.1016/j.jhazmat.2021.126735.
[56] W. Ma, N. Wang, Y. Du, P. Xu, B. Sun, L. Zhang, K.-Y.A. Lin, Human-hair-derived N, S-doped porous carbon: an enrichment and degradation system for wastewater remediation in the presence of peroxymonosulfate, ACS Sustain. Chem. Eng. 7 (2019) 2718–2727, https://doi.org/10.1021/acssuschemeng.8b05801.